Available online at www.sciencedirect.com

SciVerse ScienceDirect

Journal of the European Ceramic Society 32 (2012) 2925–2933

www.elsevier.com/locate/jeurceramsoc

Transparent alumina by vacuum sintering

Gustavo Mata-Osoro, Jose S. Moya, Carlos Pecharroman *

Instituto de Ciencia de Materiales de Madrid (ICMM), Consejo Superior de Investigaciones Científicas (CSIC), Cantoblanco, 28049 Madrid, Spain

Available online 23 March 2012

Abstract

Alumina windows transparent in IR range and translucent in UV range were obtained by high vacuum sintering ($\sim 10^{-6}$ mbar). To determine the influence of the atmosphere on grain growth, a sintering kinetics and intragranular porosity studies have been performed for samples sintered in air and in high vacuum atmospheres. It has been established that by using high vacuum sintering instead of the conventional one in air, alumina compacts with lower grain size, less impurities in grain boundaries and less quantity of intragranular pores were obtained. It has been proven that high vacuum sintering allows to reach high densities (>99%th) without exaggerated grain growth ($d_{50} < 1$ μm). Finally, strong correlation between microstructure and light transparency has been found and consequently it can be concluded that vacuum sintering clearly enhances the optical properties of alumina.

Keywords: Transparent alumina; Vacuum sintering; Light scattering; Grain growth mechanisms; Slip-cast

1. Introduction

Translucent and transparent aluminas are being investigated due to their superb mechanical properties suitable to be used for high adding value applications, such as airborne optics, windows for corrosive and hot environments and generally speaking transparent media in hostile environments.[1] However, the most relevant characteristic of transparent ceramics is the possibility to conform complex shapes avoiding expensive fabrication procedures such as single crystal growth, and machining, especially in the cases where devices with large dimensions are required.[2]

On the other hand, conventionally sintered ceramics are opaque as a consequence of the presence of different structural defects. Therefore, light scattering can be minimized or even suppressed when ceramic heterogeneities are removed or limited in concentration and size. Thus, for applications in the visible spectral range ($\lambda \sim 500$ nm) ceramics heterogeneities must be at least smaller than 50 nm but preferably shorter than 10 nm, whereas for far infrared ($\lambda \sim 5$ μm) inhomogeneities of the order of 1 μm are even tolerable.

From an electromagnetic point of view, a defect can be defined as a region with a discontinuity on the refraction index, and accordingly, the larger the difference or the extension, the larger the scattering is. In isotropic ceramic materials, the most relevant optical defects are the pores. The scattering behaviour of these defects is fully described by the Mie equation,[3] however, when the pore size is small enough, the simplest Rayleigh approximation is fair enough to fully describe the scattering mechanism.[4] Light scattering in alumina is somehow a more complex question. Due to its anisotropic character, grain scattering must also be considered. Alumina single crystals present a small difference in the refractive indices along the z direction and the xy plane, being its degree of birefringence, $\Delta n = 0.008$ or $\Delta n/n = 4.5 \times 10^{-3}$ ($n_o = 1.7638$ and $n_e = 1.7556$ at 700 nm).

The first theoretical model applied to transparent or translucent aluminas was introduced by Apetz and van Bruggen.[5] This model is basically a phenomenological modification of the Rayleigh–Gans–Debye approximation originally developed for isotropic spheres. Afterwards, a rigorous model has been developed by Pecharroman et al.[6] This model, which includes the effect of texturing in the translucency, states that light absorbance of translucent aluminas follows a λ^{-2} law and it also linearly depends on the crystallite size and on the ceramic anisotropy. This model satisfactorily reproduces the optical transmittance of some near-free porosity alumina samples presented in the literature.[5,7–16]

According to the theoretical models, in order to produce transparent aluminas porosity must be reduced to the minimum but keeping the grain size as small as possible. Thus, all transparent alumina ceramics are prepared following

* Corresponding author.
E-mail address: cpg@icmm.csic.es (C. Pecharroman).

0955-2219/$ – see front matter © 2012 Elsevier Ltd. All rights reserved.
doi:10.1016/j.jeurceramsoc.2012.02.039

specifically designed processing routes to keep porosity below 0.1% and maximum pore size below 50 nm. Consequently, it is mandatory to use no agglomerated nanometer sized alumina powders as starting material. From these powders, a green compact with a high coordination number between particles as well as a high density (>60%th), must be obtained.[13,17,18] Additionally, sintering processes must be carried out in such a manner that exaggerated grain growth will be limited to the maximum extend. Therefore, the best results for transparent alumina obtained up to now in the literature are either by spark plasma sintering (SPS)[19,20] or through wet casting, sinter in air until 96% density and subsequent HIP till all pores are eliminated.[5,21] Following these routes a RIT value of 50–60% at 650 nm can be achieved.[18]

In all the reported processing routes, a mandatory requirement is to keep the grain size as small as possible during sintering stages. Vacuum sintering is practically an unexplored technique in the literature.[22,23] While most of previous works about vacuum sintering[22,23] were performed at relatively low vacuum level (10^{-2}/10^{-3} mbar), in the present investigation, high vacuum sintering (10^{-6} mbar) have been performed to obtain transparent α-alumina ceramics. Although it is known that low vacuum ($\sim 10^{-3}$ mbar) induces a positive sintering pressure due to the removal of air and other absorbents from the pores,[24] the role of a high vacuum environment during sintering is a yet an unknown subject.[25] Under such conditions, it is expected that oxygen diffusion inside the grains of the green body may be altered as well as the level of impurities will be drastically reduced.

2. Experimental

High purity α-alumina (99.99%) (TM-DAR, Taimei Chemicals Co., Ltd.), with an average particle size of $d_{50} = 0.2$ μm, a BET specific surface area of 14.5 m^2/g and the following chemical analysis (ppm): Si (10), Fe (8), Na (8), K (3), Ca (3), Mg (2), Cu (1), Cr (<1), Mn (<1), U (<0.004), Th (<0.005) has been used as starting powder.

Powder suspensions of 60 wt% solid content were prepared using distilled water as liquid media and a 0.5 wt% addition of an alkali-free organic polyelectrolyte as surfactant (Dolapix DE-64). The pH of the obtained suspension was found to be 8.8 ± 0.1. The suspensions were homogenised by milling with alumina balls, 99.9% purity, in polyethylene containers at 150 r.p.m. for 24 h. After homogenized, the mixtures were de-aired while stirring for 1 h. The slip casting process to obtain green plates ($10 \times 10 \times 1$ mm) was performed in a pure porous alumina mould and under slight vacuum (~150 mbar) in order to eliminate bubbles.

To determine the sintering window, different dilatometric tests were done in a Bahr dilatometer with a heating rate of 5 °C/min till 1600 °C, in air and vacuum (10^{-6} mbar) environments.

The samples were sintered in an electrical controlled (±1 °C) tubular alumina (99.7% purity) furnace. This furnace has an attached vacuum system (rotatory and turbo pump) which allows to sinter to 1600 °C at 10^{-6} mbar. All the cast green plates were previously burn out at 800 °C for 24 h in air atmosphere to avoid the presence of organic residues and to eliminate the finest grains that might induce local densification, obtaining in this manner, an homogeneous microstructure.[26] Afterwards, the samples were sintered at 1350 °C, 1400 °C, 1450 °C and 1500 °C to a theoretical densities larger than 98%th. In the same way, different sintering times were employed, but, in order to simplify the exposition, only the results corresponding to the shortest (2 h)[23,27] and largest (50 h) periods will be discussed.

Sample microstructure were studied after a thermal etching (15% less than sintered temperature for one hour) on polished surfaces down to 1 μm by SEM (Hitachi, model S3000N). The grain size of the alumina was determined using the linear intercept method.[28]

Samples were prepared for analysis in a transmission electron microscope TEM (JEOL JEM 3000F) using the ion milling technique (Fischione 1010).

Sample density was measured (when applicable) by Archimedes method in distilled water.

To eliminate surface light scattering, all the sintered plates were polished on both sides. The transmittance spectra were measured using three different spectrophotometers to cover the widest possible spectral range: Nicolet 20 SXC FTIR spectrophotometer from 7 to 2.5 μm, Bruker IFS 66V FTIR from 2.5 to 0.8 μm, and finally a Jasco V660 dispersive spectrophotometer for the visible range (0.8–0.3 μm).

Bending strength, σ_f, was determined by three-point bending test and was conducted in loading direction parallel to the slip cast direction. The tests were performed at room temperature using a universal testing machine (Instron Model 4411). The specimens were loaded to failure with a cross-head speed of 0.5 mm/min and a span of 20 mm. The hardness was obtained by the Vickers indentation with a hardness indentation tester (Buehler model Micromet 5103).

3. Results

3.1. Microstructure

As can be observed in Fig. 1, all the green bodies obtained by the herewith used slip-casting procedure are constituted by a dense packing of alumina grains (with an estimated coordination number around 10, which roughly means a theoretical density in the green body of 60%) free of larges pores. The maximum size of the observed pores was found to be ~100 nm.

The shrinkage results from the dilatometer, Fig. 2a, showed that ($\Delta L/L_0$) at the end of the sintering process is higher in the case of vacuum than air sintering although the linear shrinkage rate ($d(\Delta L/L_0)/dt$) reaches a maximum at higher temperature for vacuum (1330 °C) than in the case of air sintering (1298 °C). In Fig. 2b, the theoretical densities of the alumina samples, measured by the Archimedes method, have been plotted. It should be stated that, according a simple error analysis, the estimated accuracy of this experimental procedure (~0.5%) is not enough for a precise characterization of these samples. From this plot, it can be inferred that a higher final density is obtained for air sintered samples during 2 h but, conversely, samples sintered in

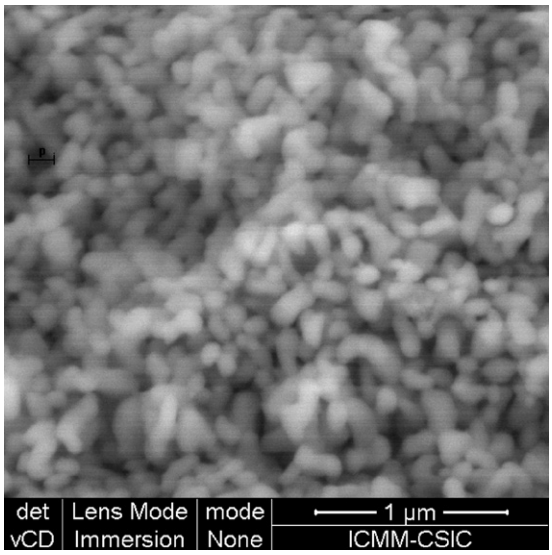

Fig. 1. SEM micrograph of the green compact presintered at 800 °C for 24 h in air.

vacuum during 50 h seem to have a slightly higher density. As expected, as long as the holding time of sintering is, as higher the density of the samples is.

According to Fig. 3a and b, the microstructures of vacuum sintered samples at 1400 °C for 2 h present a smaller average grain size than the ones sintered in air atmosphere. This tendency can be extended to most of the sintering conditions, as it appears in Fig. 3c. It is worth to note that this trend is even more pronounced for the higher sintering temperatures.

TEM micrographs corresponding to samples sintered at 1350 °C, in air and in vacuum for 50 h, are shown in Fig. 4. The most striking feature of vacuum sintering samples is the lattice matching between grains (HRTEM Fig. 4c) resembling the images of an epitaxial growth structures. In the case of air sintered samples, grain interface does not look to have some kind of lattice correspondence (Fig. 4d). Instead, a kind of crystalline disordered region seems to extend along the interfaces. Additionally, triple points corresponding to air sintered samples present a more rounded shape (Fig. 4a and b).

3.2. Mechanical properties

The Vickers hardness as a function of the grain size is plotted in Fig. 5. It can be observed that for dense samples (densities larger than 99%th) the hardness decreases with the grain size, following a Hall–Petch behaviour.[29] For samples with densities below 99%th. Vickers hardness is much smaller and dependant on porosity

The bending strength has been measured only in the sample with the highest hardness value, sintered at 1350 °C, 50 h in vacuum and the result was found to be $\sigma_f = 700 \pm 50$ MPa.

3.3. Optical properties

In Fig. 6a the transmittance of two alumina ceramics has been plotted. In order to illustrate the effect of high vacuum on

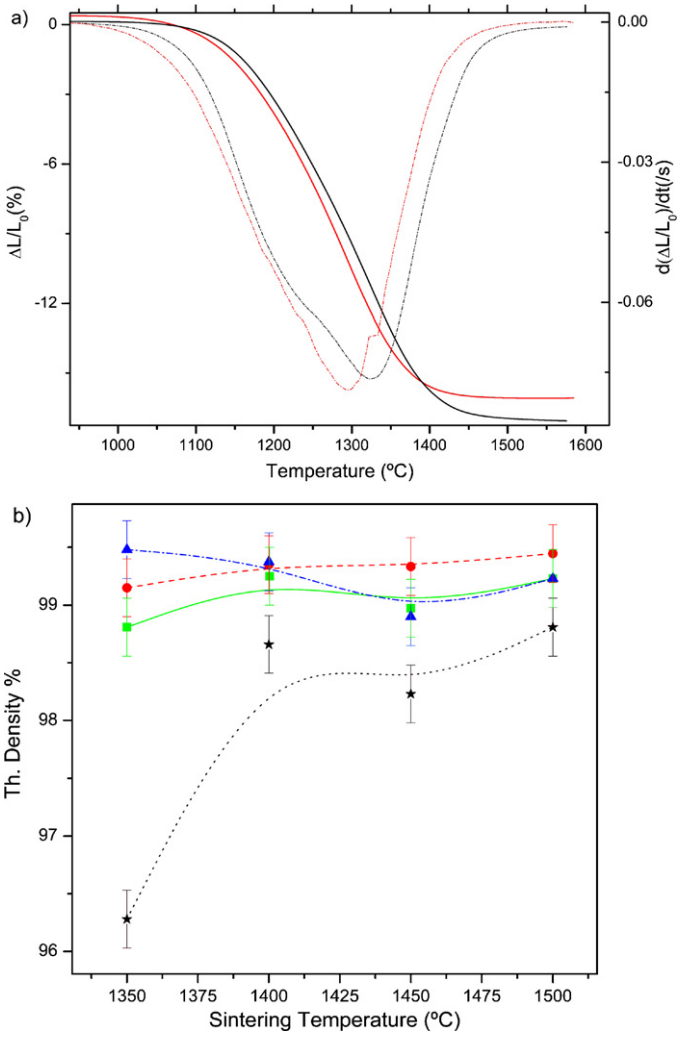

Fig. 2. (a) Dilatometer experiments performed with different atmospheres. Dash lines correspond to $d(\Delta L/L_0)/dt$, red in air and black in vacuum. Solid lines correspond to $\Delta L/L_0$, red in air and black in vacuum. (b) Archimedes density vs. sintering temperature where black stars are 2 h vacuum sintering, green squares are 2 h air sintering, blue triangles are 50 h vacuum sintering, red dots are 50 h air sintering. (For interpretation of the references to color in this figure legend, the reader is referred to the web version of the article.)

sintering, we have chosen the most transparent sample which was obtained at 1350 °C for 50 h in high vacuum conditions and its counterpart processed under the same conditions but in air. The vacuum sintered sample presents a spectral window which approximately extends from 6500 to 700 nm. The air sintered sample displays a poor transmittance, smaller than a half of the vacuum sample. Additionally, the spectral window of this later is narrower, especially in the visible range.

4. Discussion

It has been previously reported that sintering under low vacuum ($\sim 10^{-3}$ mbar) conditions induces a positive sintering pressure due to the removal of air and other absorbents from the pores.[22] However, according to our experiments we did not find any noticeable effect of low vacuum on transparent aluminas, probably due to the high density of the studied samples. Instead,

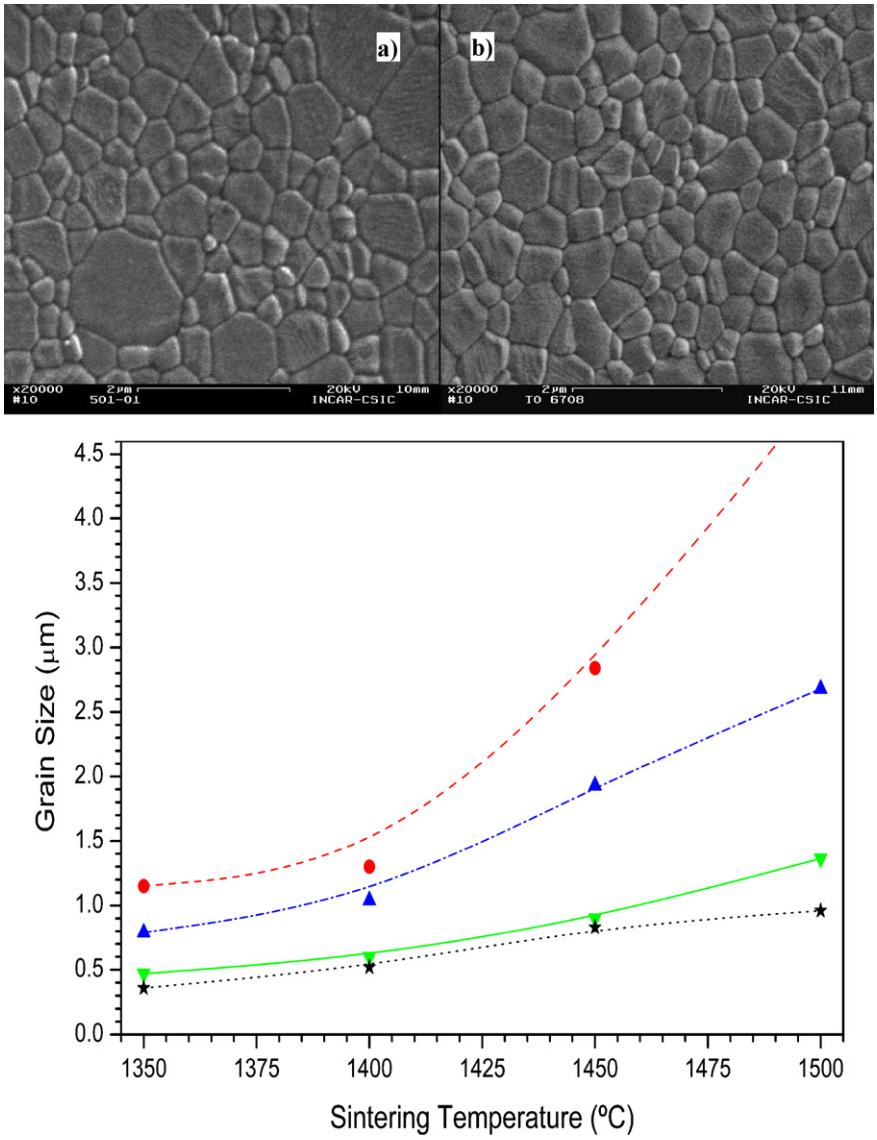

Fig. 3. (a) SEM image of sample sintered at 1400 °C for 2 h in air. (b) SEM image of sample sintered at 1400 °C for 2 h in vacuum. (c) Grain size (d_{50}) vs. sintering temperature where black stars are 2 h vacuum sintering, green down triangles are 2 h air sintering, blue up triangles are 50 h vacuum sintering, red dots are 50 h air sintering. (For interpretation of the references to color in this figure legend, the reader is referred to the web version of the article.)

high vacuum sintering ($\sim 10^{-6}$ mbar) revealed to have a strong effect in the optical quality of resulting ceramics.

One of the most determinant factors which determine the grain growth mechanism is the presence of impurities in the green body during the sintering process. It is well known traces of Si, Ca, K, Mg. etc., could be incorporated during the powder processing stages or volatilized from the furnace during sintering. It should be noted, that in order to avoid sample contamination, the slip-casting was performed in a semi-clean room using an alumina mould instead of the classical plaster one and the tubular furnace was a monolithic piece of high purity alumina.

In the case of air sintered samples there are two impurities sources: the first are some traces from the tubular alumina furnace and the second is the water vapour present in the atmosphere. In the case of high vacuum sintering (high vacuum $<10^{-6}$ mbar) the continuous pumping remove all the atomic species from the oven so that contamination of the samples is practically avoided.

However the observed effect on the grain growth of the sintering atmosphere is not the expected one according to the theoretical predictions.[30] It is commonly found that impurities reduce the mobility of the grain boundary, acting as solute or precipitating at the grain boundaries causing a pinning effect. In our case, air sintered samples (richer in impurities) present a bigger grain size than the vacuum sintered ones. In fact, the TEM micrograph, Fig. 4c and d, show a clean grain boundary in the vacuum sintered sample and an amorphous grain boundary in the air sintered. This amorphous grain boundary has been observed previously by different authors.[31,32]

In our particular case, several factors can explain the smaller average grain size of vacuum sintered samples versus the air sintered ones. In the first place, a very low oxygen partial pressure, (pO_2) could depletes the oxygen diffusion through the

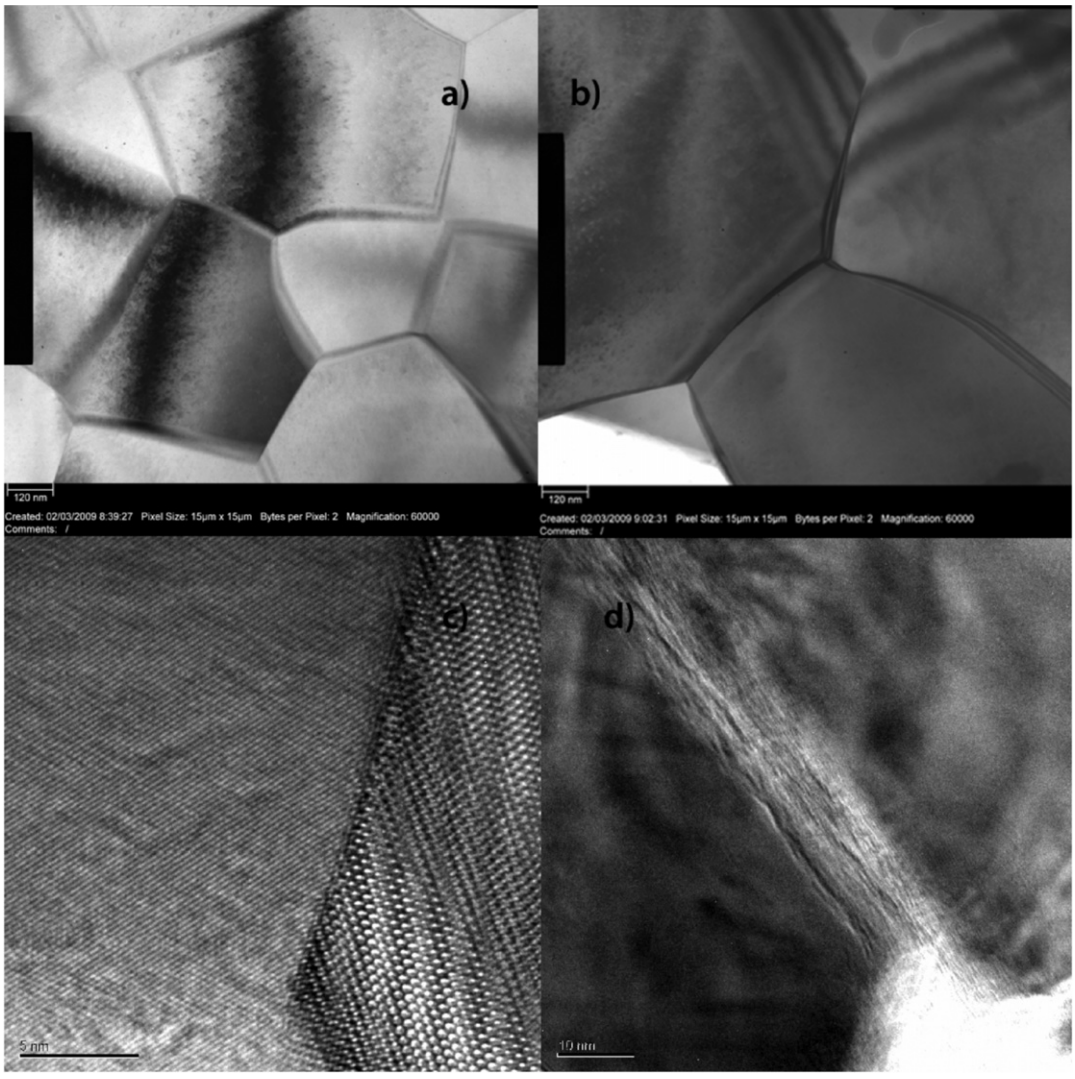

Fig. 4. (a) TEM image of sample sintered at 1350 °C for 50 h in vacuum. (b) TEM image of sample sintered at 1350 °C for 50 h in air. (c) TEM image of sample sintered at 1350 °C for 50 h in vacuum. (d) TEM image of sample sintered at 1350 °C for 50 h in air.

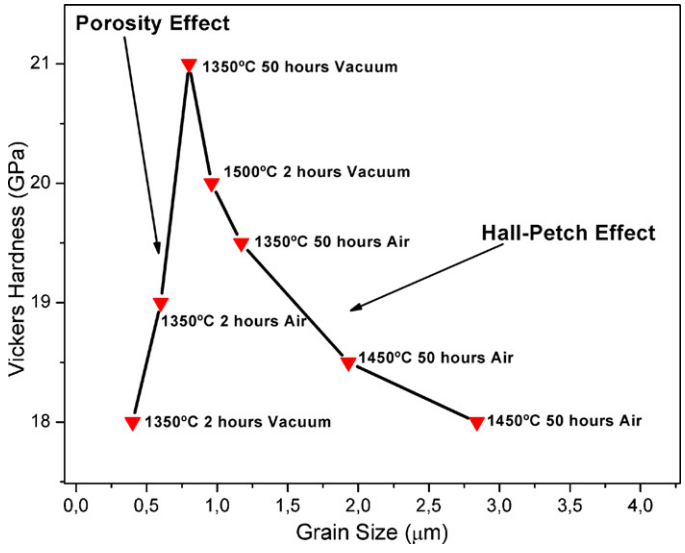

Fig. 5. Vickers hardness vs. grain size of representative samples.

grain boundary limiting its mobility. According to Bennison and Harmer[33] the intrinsic motion of a grain boundary in a pure system (as it is our case) is determined by the diffusional transfer of matter from the contracting grain to the expanded grain. That is, the mobility of the grain boundary is proportional to the diffusion coefficient. This diffusion coefficient is depleted at very low pO_2. On the other hand, Wei and Rhodes[34] and Chinelatto and Tomasi[25] have reported that water vapour affects the mass transport and consequently increases the sintering and grain growth, in air atmosphere. This is in perfect agreement with our experimental results. However for a fully understanding of the operating diffusions mechanisms more research has to be done.

Referring to the optical properties, as a consequence of the higher grain side of the air sintered samples, entrapment of pores have taking place as can be deduced from microstructural observation (Fig. 3a and b) and from the dilatometric curve (Fig. 2a) where the final shrinkage is about 0.6% higher in vacuum than in air. Furthermore the linear shrinkage rate ($d(\Delta L/L_0)/dt$) is maximal for lower temperatures in air than in vacuum (Fig. 2a). Thus,

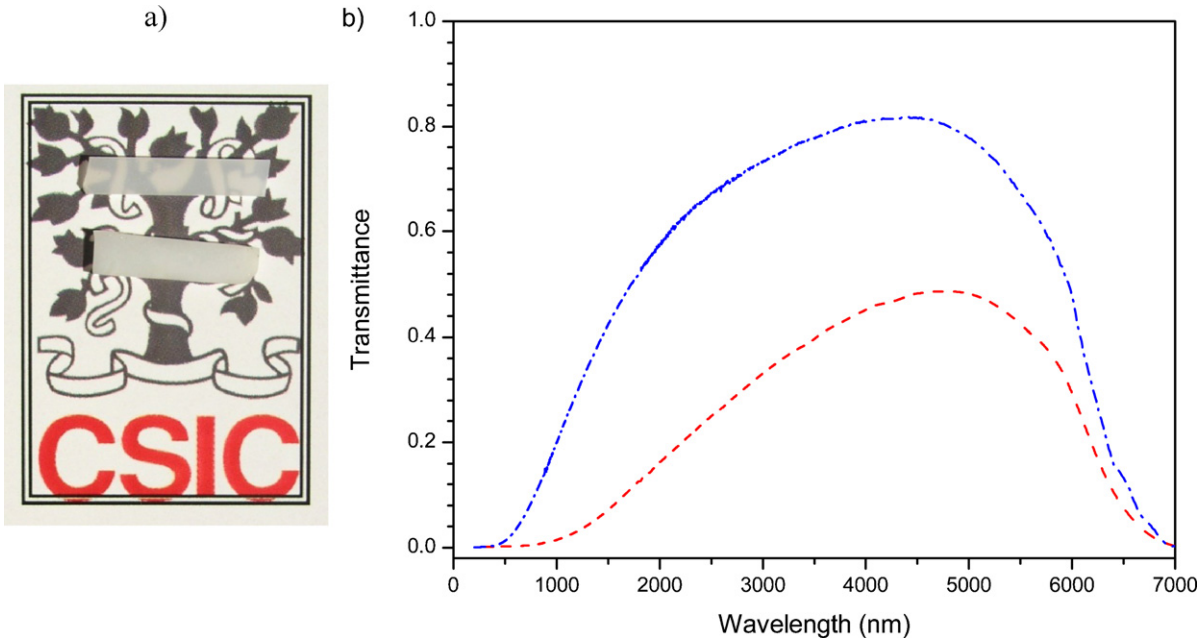

Fig. 6. (a) External aspect of the samples sintered at 1350 °C for 50 h in vacuum top side and in air bottom side. (b) Experimental optical transmittance vs. wavelength, of samples sintered at 1350 °C for 50 h in vacuum blue dash dot line and in air 50 h red dash line. (For interpretation of the references to color in this figure legend, the reader is referred to the web version of the article.)

for lower sintering times (2 h), the obtained density is smaller in vacuum than in air (Fig. 3c), after longer periods (50 h), the observed density is the opposite (Fig. 3c).

Because vacuum samples require longer times to totally remove the porosity, it is easier to determine the optimal conditions (temperature and sintering time) for achieving a near 100%th density while keeping a homogeneous grain size distribution. Therefore, best results were obtained for long times (50 h) at a sintering temperature close to the one of maximum shrinkage rate.

One of the main conclusions we can drawn from the microstructural analysis of different transparent ceramics is the extreme level of perfection they exhibit. Moreover, the practical total absence of porosity and the high degree of stability of grain interfaces in high vacuum sintered aluminas complicates even more a precise microstructural analysis. In this regard we want to point out that a simple analysis of the absorbance curves allows determining which the main source of scattering is. This information is crucial, because once the most relevant defect is found several strategies can be implemented in order to avoid it in the next fabrication batch.

Optical properties are strongly determined by the pore and grain size distribution. In both cases, two scattering mechanisms should be applied.

$$R.I.T. = \left[1 - 2\left(\frac{n-1}{n+1}\right)^2\right] e^{-\kappa d} = T_0 e^{-A} \tag{1}$$

where A is the total absorbance, n the refractive index of the sample, d its thickness and κ the linear absorption coefficient. The absorbance has three relevant terms:

$$A = A_p + A_g + A_{da} \tag{2}$$

A_p, A_g and A_{da} stand for pore, grain and anomalous scattering terms. Absorbance can be calculated through this relationship which relates it with the efficiency scattering factor Q_{ext}.

$$A = \frac{3}{4} f Q_{ext} d \tag{3}$$

where f is the volume defect concentration.

As it has been previously stated, the pore scattering mechanism can be approximated by the Rayleigh model. The analytical efficiency scattering factor and absorbance expression is given by:

$$Q_{\text{Rayleigh}} = \frac{128}{3}\pi^4 \frac{\langle a_p^4 \rangle}{\lambda^4} \left| \frac{1 - \langle n \rangle^2}{1 + 2\langle n \rangle^2} \right|^2 \tag{4}$$

$$A_p = 32\pi^4 f_p \frac{\langle a_p^3 \rangle}{\lambda^4} \left| \frac{1 - \langle n \rangle^2}{1 + 2\langle n \rangle^2} \right|^2 d \tag{5}$$

This is a very interesting expression, because it states that porosity (f_p) and medium pore size $\langle a_p^3 \rangle$ will be keep as small as possible. In fact, the absorbance for slightly porous aluminas is mainly determined by the coefficient $\langle a_p^3 \rangle f_p/\lambda^4$. Therefore, only samples with small values of $\langle a_p^3 \rangle f_p$ will present appreciable transmittances at visible wavelengths. It should be noted, that because of the definition of $\langle a_p^3 \rangle$

$$\langle a_p^3 \rangle = \sum_i a_i^3 f_{p,i} = \frac{\sum_i a_i^6}{\sum_i a_i^3} \tag{6}$$

It is easy to show that $\langle a_p^3 \rangle > \langle a_p \rangle^3$. In fact, $\langle a_p^3 \rangle$ is closer to the maximum detected pore radius, so that in a very good approximation, this average value can be substituted by the maximum pore size found. In this sense it is clear the need of a very

good processing and sintering that avoids the presence of large porosity, even if they are scarce.

In case that pore size is much larger than the incident wavelength, efficiency scattering section reaches a constant value of $Q_{ext} = 2$, so that the absorbance is given by:

$$A_p = \frac{3}{2}\frac{f_p d}{\langle a_p \rangle} \quad \text{if} \quad \lambda \ll \langle a_p \rangle \tag{7}$$

Grain and pore light scattering can have a similar weight in the case of transparent alumina ceramics in the visible range. The grain scattering model uses the Rayleigh–Gans–Debye approximation. This is valid for small scatters with a refractive index very similar to that of the environment ($|m-1| \ll 1$ and $2\pi|m-1|a_g/\lambda \ll 1$), where m is the quotient between the refractive index of the scatter and that of the surrounding medium, a_g the grain radius and λ the incident wavelength. The model states that transmittance of dense alumina ceramics basically depends not only on the maximum grain size but also on the preferential orientation of their c-axis, or texture. This model predicts an absorbance law following:

$$A_g = -\frac{6\pi^2 \langle a_g \rangle}{\lambda^2}\left(\frac{\Delta n}{\langle n \rangle}\right)^2 \alpha(\xi) d \tag{8}$$

where Δn is the difference between the refraction index in the different axis and equals to 0.008 for α-alumina and d is the thickness of the sample. Thus, if the samples are near-free porosity, the slope of the line is proportional to the values of the texture function $\alpha(\xi)$, where ξ is the effective angle of the optical axis of a singular crystallite with the sample surface normal and $\langle a_g \rangle$, the average grain radius value corresponding to a volume grain distribution, defined by:

$$\langle a_g \rangle = \sum_i a_{g,i} f_{g,i} = \frac{\sum_i a_{g,i}^4}{\sum_i a_{g,i}^3} \tag{9}$$

As it happens in the case of the pore size distribution, it can be stated, that with a good degree of approximation, for heterogeneous grain size distribution, $\langle a_g \rangle$ can be considered similar to the maximum value of grain radius experimentally found.

The anomalous diffraction term[4] appears when grain size is larger than wavelength but keeping contrast small. In fact, this term can be seen as the upper limit of the grain scattering. In a similar way as it happens with pore scattering, in case of large particle size, the scattering efficiency factor tends to $Q_g = 2$[4] so that the absorptions can be approximately written as:

$$A_{ad} \cong \frac{3d}{2\langle a_g \rangle} \quad \text{if} \quad \lambda \ll \langle a_g \rangle \tag{10}$$

Therefore, in case of aluminas with moderate to low porosity and grain size, the transmittance is given by

$$A = -\log(T_0) + A_p + A_g \tag{11}$$

$$A_p = \begin{cases} 32 f_p \pi^4 \left|\dfrac{n^2-1}{n^2+2}\right|^2 \dfrac{\langle a_p^3 \rangle}{\lambda^4} d & \text{if} \quad \lambda > \langle a_p \rangle \\ \dfrac{3}{2}\dfrac{d}{\langle a_p \rangle} f_p & \text{if} \quad \ll \langle a_p \rangle \end{cases} \tag{12}$$

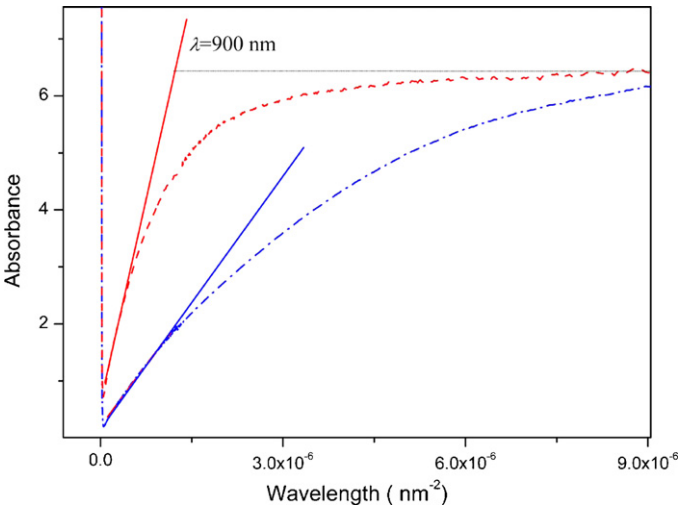

Fig. 7. Logarithm of transmittance (absorbance) vs. the inverse of the wavelength square of samples sintered at 1350 °C for 50 h in vacuum blue dash dot line and in air 50 h red dash line. Straight lines represent the linear fitting in the low wavelength region. (For interpretation of the references to color in this figure legend, the reader is referred to the web version of the article.)

$$A_g = \begin{cases} 6\pi^2 \Delta n^2 \alpha(\xi) \dfrac{\langle a_g \rangle}{\lambda^2} d & \text{if} \quad \lambda > \langle a_g \rangle \\ \dfrac{3}{2}\dfrac{d}{\langle a_g \rangle} & \text{if} \quad \lambda \ll \langle a_g \rangle \end{cases} \tag{13}$$

These expressions state that depending on the scattering defect, the absorbance curve presents different characteristics. In the case of pore-free transparent aluminas, absorbance (or $-\log(T)$) follows a $1/\lambda^2$ behaviour in a broad range of wavelengths. For pore free with large grain ceramics, the former straight line saturates for shorter wavelengths as a consequence of anomalous diffraction. Finally, if dense alumina presents low porosity and small grain size, the linear behaviour of absorbance vs. $1/\lambda^2$ transforms into a parabolic profile for short wavelengths.

This simple rule has been applied to determine the main source of scattering of alumina ceramics.[6,12,35] In the case of the sample sintered at 1350 °C for 50 h in vacuum (Fig. 7), a linear regime can be found for longer wavelengths, to saturate around optical wavelengths. It clearly indicates that alumina grains have grown enough to scatter following the anomalous diffraction regime. If we focus on the linear regime, the absorbance data can be fitted to nearly isotropic alumina, i.e. $\alpha(\xi) = 0.35$[6] resulting a maximum grain size of $a_g = 1830$ nm, in good agreement with the experimental results. It should be noted that although this grain size induces a large grain scattering, the limiting nature of anomalous diffraction makes possible that this sample presents an acceptable level of transparency even to 500 nm (Fig. 6).

In the case of air sintered sample, one can suppose at first sight that this sample presents a similar behaviour as the previous one. i.e. $1/\lambda^2$ regime for longest wavelengths followed by a saturation for wavelengths shorter than 900 nm. However a detailed analysis of the air sintered sample curve reveals that it does not cross the coordinate axis at $-\log(T_0)$ for $1/\lambda^2 = 0$ as it predicts the theory. It should be reminded that the former model always assumes that the scattering efficiency is low. In the case

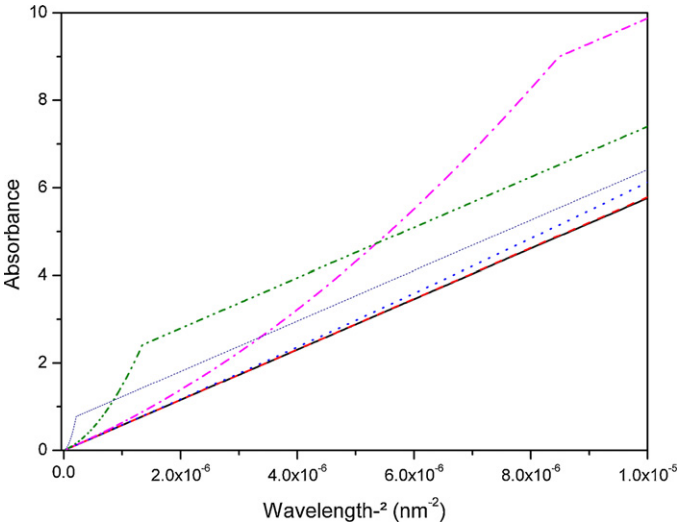

Fig. 8. Absorbance model of polycrystalline alumina with grain radius $a_g = 1000$ nm, thickness 1 mm and porosity $f_p = 5 \times 10^{-3}$ for different pore radius ($a_p = 5$, 12.5, 31.5, 79.2, 200 and 500 nm are black solid, red dash, blue dot, magenta dash dot, dash dot dot and short dashed respectively). (For interpretation of the references to color in this figure legend, the reader is referred to the web version of the article.)

of large porosity, approximations are no longer valid, so that full Mie calculations should be carried out to fully describe the transmittance curves. Fig. 8 simulates the absorption curves vs. $1/\lambda^2$ for 1 μm alumina grains ceramic containing pores with different size. For very small porosity ($a_p < 15$ nm), defects have no effect on absorbance. For moderate pore size ($15 < a_p < 200$ nm) absorbance curve presents a parabolic shape, as it corresponds to the Rayleigh regime. Finally if pore size is large enough ($a_p > 200$ nm) the pore contribution to absorbance appear as constant value (wavelength independent) that shifts up the whole curve. As a result, the extrapolation of the linear regime does not crosses at $-\log(T_0)$ for $1/\lambda^2 = 0$ as it appears in Fig. 7 for the air sintered sample. Therefore, it can be concluded that sample sintered in air contains large pores (~200 nm). This agrees with the observed result that the grain microstructure obtained by vacuum sintering is more homogeneous than the one prepared in air atmosphere. Therefore, the role of vacuum sintering is to inhibit the exaggerated grain growth. It could indicate a poorer degree of sintering for short times. However, for larger times, this limited growth rate allows a controlled way to remove the green body porosity.

In summary, it can be stated that vacuum sintering at very low pressures (~10^{-6} mbar) slows down the sintering rate, hindering both, exaggerated grain growth and intragranular porosity. Thus, alumina compacts with very low and small porosity and grain size can be simultaneously obtained by sintering for long periods of time (50 h) at the temperature of maximum shrinkage rate. Vacuum sintered samples present high transmittances over a wide spectral window. Besides, a simple analysis of the absorbance curve vs. for $1/\lambda^2$ allows to determine the most relevant scattering mechanism: (i) small grain scattering (straight line); (ii) small porosity (parabolic curve); (iii) large grain scattering (constant or saturation of absorbance); (iv) large porosity (curve does not extrapolate at $-\log(T_0)$ for $1/\lambda^2 = 0$). It is worth to remark that the same ceramic properties that make transparent samples, are the ones required for high hardness and bending strength values. Particularly, hardness of $H_V = 21 \pm 1$ GPa and bending strength of $\sigma_f = 700 \pm 50$ MPa has been measured in the most transparent sample (1350 °C, 50 h in vacuum).

References

1. Wei GC. Transparent ceramic lamp envelope materials. *J Phys D: Appl Phys* 2005;**38**(17):3057–65.
2. Cain M, Morrell R. Nanostructured ceramics: a review of their potential. *Appl Organomet Chem* 2001;**15**(5):321–30.
3. Bohren CF, Huffman DR. *Absorption and scattering of light by small particles*. Wiley; 1983.
4. Hulst HC. *Light scattering by small particles*. Wiley; 1957.
5. Apetz R, van Bruggen MPB. Transparent alumina: a light-scattering model. *J Am Ceram Soc* 2003;**86**(3):480–6.
6. Pecharroman C, Mata-Osoro G, Diaz LA, Torrecillas R, Moya JS. On the transparency of nanostructured alumina: Rayleigh–Gans model for anisotropic spheres. *Opt Expr* 2009;**17**(8):6899–912.
7. Bernard-Granger G. Influence of MgO or TiO_2 doping on the sintering path and on the optical properties of a submicronic alumina material. *Scr Mater* 2007;**56**(11):983–6.
8. Jiang D. Optically transparent polycrystalline Al_2O_3 produced by spark plasma sintering. *J Am Ceram Soc* 2008;**91**(1):151–4.
9. Krell A, Klimke J. Effects of the homogeneity of particle coordination on solid-state sintering of transparent alumina. *J Am Ceram Soc* 2006;**89**(6):1985–92.
10. Li JG, Ye YP. Densification and grain growth of Al_2O_3 nanoceramics during pressureless sintering. *J Am Ceram Soc* 2006;**89**(1):139–43.
11. Shen ZJ, Johnsson M, Zhao Z, Nygren M. Spark plasma sintering of alumina. *J Am Ceram Soc* 2002;**85**(8):1921–7.
12. Alvarez-Clemares I, Mata-Osoro G, Fernandez A, Lopez-Esteban S, Pecharroman C, Palomares J, et al. Transparent alumina/ceria nanocomposites by spark plasma sintering. *Adv Eng Mater* 2010;**12**(11):1154–60.
13. Aman Y, Garnier V, Djurado E. Influence of green state processes on the sintering behaviour and the subsequent optical properties of spark plasma sintered alumina. *J Eur Ceram Soc* 2009;**29**(16):3363–70.
14. Dang KQ, Takei S, Kawahara M, Nanko M. Pulsed electric current sintering of transparent Cr-doped Al_2O_3. *Ceram Int* 2010;**37**(3):957–63.
15. Gandhi AA, Gunning RD, Ryan KM, Tofail SAM. The role of texturing and densification on optical transmittance of hydroxyapatite ceramics. *J Am Ceram Soc* 2010;**93**(11):3773–7.
16. Kim BN, Hiraga K, Morita K, Yoshida H, Kagawa Y. Light scattering in MgO-doped alumina fabricated by spark plasma sintering. *Acta Mater* 2010;**58**(13):4527–35.
17. Bowen P, Carry C. From powders to sintered pieces: forming, transformations and sintering of nanostructured ceramic oxides. *Powder Technol* 2002;**128**(2–3):248–55.
18. Krell A, Blank P, Ma HW, Hutzler T, Nebelung M. Processing of high-density submicrometer Al_2O_3 for new applications. *J Am Ceram Soc* 2003;**86**(4):546–53.
19. Stuer M, Zhao Z, Aschauer U, Bowen P. Transparent polycrystalline alumina using spark plasma sintering: effect of Mg, Y and La doping. *J Eur Ceram Soc* 2010;**30**(6):1335–43.
20. Grasso S, Kim B-N, Hu C, Maizza G, Sakka Y. Highly transparent pure alumina fabricated by high-pressure spark plasma sintering. *J Am Ceram Soc* 2010;**93**(9):2460–2.
21. Pecharroman C. Determination of texture by infrared spectroscopy in titanium oxide-anatase thin films. *J Appl Phys* 2003;**93**(8):4634–45.
22. Handwerker CA, Dynys JM, Cannon RM, Coble RL. Dihedral angles in magnesia and alumina – distributions from surface thermal grooves. *J Am Ceram Soc* 1990;**73**(5):1371–7.

23. Hotta Y, Banno T, Oda K. Physical properties of slip casting of high pure Al_2O_3 slurry using porous Al_2O_3-glass mold. *J Mater Sci* 2002;**37**(2):417–23.
24. Srdic VV, Winterer M, Hahn H. Sintering behavior of nanocrystalline zirconia prepared by chemical vapor synthesis. *J Am Ceram Soc* 2000;**83**(4):729–36.
25. Chinelatto ASA, Tomasi R. Influence of processing atmosphere on the microstructural evolution of submicron alumina powder during sintering. *Ceram Int* 2009;**35**(7):2915–20.
26. Lin FJT, de Jonghe LC, Rahaman MN. Microstructure refinement of sintered alumina by a two-step sintering technique. *J Am Ceram Soc* 1997;**80**(9):2269–77.
27. Krell A, Blank P. Grain-size dependence of hardness in dense submicrometer alumina. *J Am Ceram Soc* 1995;**78**(4):1118–20.
28. Mendelson MI. Average grain size in polycrystalline ceramics. *J Am Ceram Soc* 1969;**52**(8):443–6.
29. Pande CS, Cooper KP. Nanomechanics of Hall–Petch relationship in nanocrystalline materials. *Progr Mater Sci* 2009;**54**(6):689–706.
30. Thompson AM, Harmer MP. Influence of atmosphere on the final-stage sintering kinetics of ultra-high-purity alumina. *J Am Ceram Soc* 1993;**76**(9):2248–56.
31. Moya JS, Kriven WM, Pask JA. Influence of grain boundary silica impurity on alumina toughness. In: Pask JA, Evans AG, editors. *Mater Sci Res, 14: Surfaces and Interfaces in Ceramic and Ceramic-Metal Systems. Plenum Press*. 1981. p. 317–226.
32. MacLaren I, Cannon RM, Gülgün MA, Voytovych R, Popescu-Pogrion N, Scheu C, et al. Abnormal grain growth in alumina: synergistic effects of yttria and silica. *J Am Ceram Soc* 2003;**86**(4):650–9.
33. Bennison SJ, Harmer MP. Swelling of hot-pressed $A1_2O_3$. *J Am Ceram Soc* 1985;**68**(11):591–7.
34. Wei GC, Rhodes WH. Sintering of translucent alumina in a nitrogen–hydrogen gas atmosphere. *J Am Ceram Soc* 2000;**83**(7): 1641–8.
35. Alvarez-Clemares I, Mata-Osoro G, Fernandez A, Lopez-Esteban S, Pecharroman C, Torrecillas R, et al. Ceria doped alumina by Spark Plasma Sintering for optical applications. *J Eur Ceram Soc* 2012;**32**(11):2917–24.